Fundamental study of the effect of particle size distribution and shape of sand on the angle of repose test results

E. Kamegaya
Graduate School of Science and Engineering, Chuo University, Tokyo, Japan
H. Nishioka
Department of Civil and Environmental Engineering, Chuo University, Tokyo, Japan

ABSTRACT

In sandy soils, the angle of internal friction (ϕ) is a key parameter influencing resistance force during construction activities. Enhancing the precision of ϕ value estimation, derived from standard penetration test (SPT) N-values, is beneficial for planning cost-effective and efficient construction projects. The current statistical relationship between SPT N-values and their estimation equations exhibits significant variations. This study aims to augment the accuracy of these estimations by incorporating angle of repose data into the equations based on SPT N-values. The primary objective was to elucidate the effect of particle size distribution and particle shape on the repose angle after avalanching (α_R) in the emission method. The investigation revealed that, in terms of particle size distribution, α_R tended to be higher for samples containing a higher proportion of small-sized particles, with the exception of certain characteristic samples. An analysis of the influence of particle shape revealed that α_R for spherical samples was consistently low relative to nonspherical samples. Intriguingly, samples with nearly identical aspect ratios (AR), a shape indicator, displayed varying α_R values. This suggests that the angle of repose is influenced not only by density, particle size distribution, and particle shape but also by additional factors, including surface roughness.

Key words: *Angle of repose, Particle size distribution, Particle shape, Toyoura sand, Glass beads*

1. Introduction

In the press-in construction method, accurately predicting the resistance force is crucial for selecting an appropriate machine during the planning phase. In sandy soil, this resistance force is predominantly governed by the angle of internal friction (ϕ). The ϕ value is a key in determining soil resistance to shear forces, thereby influencing aspects such as slope stability, foundation design, and the stability of retaining walls. Accurate ϕ values are indispensable for ensuring structural integrity and safety in engineering projects involving granular materials. However, estimating ϕ typically necessitates costly soil-sampling methods to secure undisturbed samples. It is necessary to conduct laboratory tests such as triaxial compression test on the undisturbed samples. Thus, the present practical method for determining ϕ values is based on a direct statistical relationship with the N-values obtained from a standard penetration test (SPT).

The SPT N-values are related to the relative density (D_r) and ϕ, an indicator that is also affected by the effective overburden pressure (σ_v'). **Eqs. (1)** (Meyerhof, 1956)**, (2)** (Schultze and Menzenbach, 1961)**,** and **(3)** (Yoshida and Kokusho, 1988) show the equations for D_r [%] and SPT N-values considering σ_v' values [kN/m^2]. **Eq. (3)** is for dense gravelly soils with a maximum particle size of 50 mm or less.

$$D_r = 208\sqrt{\frac{N}{\sigma_V' + 69}} \quad (1)$$

$$\log_e D_r = 0.478 \log_e N - 0.262 \log_e (0.01\sigma_V') + 2.84 \quad (2)$$

$$D_r = 25.7 N^{0.43} \cdot \sigma_V'^{-0.1} \quad 50 \le \sigma_V' \le 6000 \quad (3)$$

Eqs. (4) (Japanese Road Association, 2002)**, (5)** (The Japan Harbor Transportation Association, 1999)**, (6)** (Railway Technical Research Institute, 2000)**,** and **(7)** (Architectural Institute of Japan, 2001) show the equations for ϕ and SPT N-values considering σ_v' values used in each Japanese standard.

$$\phi = 4.8 \ln\left(\frac{170N}{\sigma_V' + 70}\right) + 21 \quad (N > 5) \quad (4)$$

$$\phi = 25 + 3.2\sqrt{\frac{100N}{70 + \sigma_V'}} \quad (5)$$

$$\phi = 1.85\left(\frac{N}{0.01\sigma_V' + 0.7}\right)^{0.6} + 26 \quad (6)$$

$$\phi = 0.5N + 24 \quad \text{(upper limit for earthquake)}$$

$$\phi = \sqrt{20N_1} + 20 \quad (3.5 \le N_1 \le 20)$$
$$\phi = 40 \quad (20 < N_1) \quad (7)$$
$$N_1 = \sqrt{9.8 / \sigma_V'} \times N$$

Thus, there are multiple estimating equations corresponding to the SPT N-values and ϕ, which means that significant variations are present in the statistical correlations. Refining the ϕ estimate from SPT N-values is integral for planning more cost-effective and efficient construction projects.

To address this, our study aims to enhance the accuracy of these estimations by incorporating angle of repose data into the SPT N-value-based equations. The angle of repose, which reflects the mechanical behavior of sand, is sometimes assumed to be equivalent to the ϕ values and can be conveniently measured, even in disturbed samples.

A previous study (Kwag et al. 1998) examined the relationship between angle of repose and the ϕ value, without considering density. In the emission method, which is a type of angle of repose test, the angle of repose is the angle of slope created by the collapse of the sample when it is emitted from the container.

The proposed emission method (Kamegaya and Nishioka, 2023) utilizes a modified version of the mold and collar used in the JIS A 1224 standards for determining the minimum and maximum densities of sands based on the reference of Nakata et al (2022). The proposed emission method can accurately measure the density of sand. A previous study established the usefulness of the emission method, which is a newly developed test for determining the angle of repose. The repose angle after avalanching (α_R) was shown to increase with the increase in relative density (D_r).

The gradient of this trend was less steep for spherical glass beads and steeper for angular river sand, indicating the influence of particle shape. However, the above study did not incorporate quantitative parameters for particle shape. Further, the effect of diverse particle shapes on the angle of repose were not explored. Matsuoka et al. (2003) demonstrated that ϕ is significantly influenced by particle shape, degree of irregularity, and D_r . Thus, the existence of a similar tendency for the particle shape to affect the angle of repose must be examined.

In the distinct element method, the angle of repose is more than 10° higher for nonspherical particles than for spherical particles (Maeda et al. 2015), which confirms that particle shape has a significant effect on the angle of repose.

This study implemented an emission method focusing on particle size distribution and shape to examine their effects on α_R. Specifically, the emission method was modified with a collar height of 60 mm to observe conical slopes. The impact of particle size distribution was analyzed through sieve analysis within the same sample. To assess the influence of particle shape, four samples with varying shapes, while approximating particle size distribution, were utilized. The aspect ratio (AR) was used as a quantitative measure of particle shape. This report specifically discusses α_R at minimum density.

Matsukura and Onda (1989) distinguished two types of angle of repose: the critical angle of repose (α_C) and the repose angle after avalanching (α_R). The emission method can only measure the repose angle after avalanching (α_R).

2. Materials and Methods

2.1. Samples and their physical properties

This experiment involved dry soil samples, encompassing Toyoura sand (Ts), two varieties of mountain sand (Ms1, Ms2), two types of river sand (Rs1, Rs2), and spherical glass beads (Gb1, Gb2). All these samples were classified as sand (S) according to the JGS 0051-2009 standard for the classification of geomaterials for engineering purposes. In this study, Ms2, Rs2, and Gb2 were subjected to sieving to alter their particle size and were blended to approximate the Ts particle size distribution. Sieve openings of 0.075, 0.106, 0.25, 0.425, 0.85, and 2 mm were utilized, and all samples were 2 mm or less in diameter.

Regarding the glass beads, Gb1 comprised a mix of beads measuring 0.5 mm and 1.0 mm in diameter. By contrast, Gb2 included a blend of beads with diameters of 0.090–0.106, 0.150–0.180, 0.250–0.355, and 0.5 mm. **Fig. 1** illustrates the particle size distribution curves for all seven samples. Additionally, **Table 1** presents the specifications of the sand samples, including their uniformity coefficient (U_c) and coefficient of curvature (U_c'). These parameters provide insights into the granularity of the sands, which is essential for understanding their behavior in various engineering applications.

Being the ratio of the major axis to the minor axis when fitting a particle to an ellipse, the aspect ratio (AR) serves as a quantitative indicator of particle shape. However, in this study, the depth-length of the particles was not measured due to the utilization of enlarged images for measurement. A perfect sphere, which facilitates easy rolling of particles, has an AR of 1.0. AR is a crucial measure of a particle's rolling resistance: a higher AR signifies increased difficulty in rolling.

In this experiment, all glass beads were deemed spherical with an AR of 1.0. For Toyoura (Ts), mountain (Ms1 and Ms2), and river sands (Rs1 and Rs2), the AR was determined by tracing the shapes of over 20 randomly selected particles. The average values of AR for these samples are presented in **Table 2**. **Fig. 2** presents enlarged images of the sand particles, highlighting their varied shapes for each sample.

The AR values for Toyoura, mountain, and river sands deviated from 1.0, implying their reduced tendency to roll. The ARs of Ts, Ms2, and Rs2 were recorded at 1.47, implying no significant variation among them.

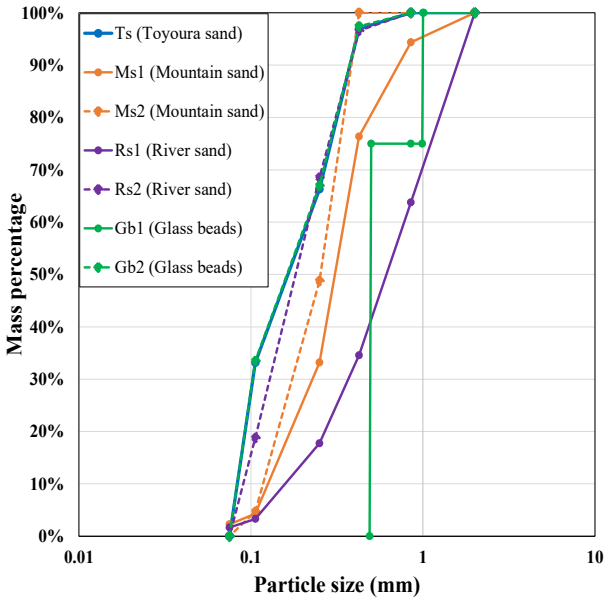

Fig. 1 Particle size distribution curves.

Table 1 D_n (n % diameter on the particle size diagram), uniformity coefficient (U_c), and coefficient of curvature(U_c').

	D_{10}	D_{30}	D_{50}	D_{60}	D_{80}	Uc	Uc'
Ts	0.083	0.104	0.165	0.218	0.320	2.627	0.598
Ms1	0.130	0.240	0.300	0.335	0.500	2.577	1.323
Ms2	0.118	0.175	0.255	0.284	0.350	2.407	0.914
Rs1	0.170	0.370	0.610	0.760	1.260	4.471	1.060
Rs2	0.092	0.129	0.185	0.218	0.315	2.370	0.830
Gb1	0.500	0.500	0.500	0.500	1.000		
Gb2	0.083	0.104	0.165	0.218	0.317	2.627	0.598

Table 2 Average (AVE) of aspect ratio (AR), standard deviation (SD), and coefficient of variation (CV).

AR	AVE	SD	CV
Ts	1.467	0.366	24.94%
Ms1	1.425	0.223	15.66%
Ms2	1.470	0.304	20.71%
Rs1	1.521	0.482	31.67%
Rs2	1.486	0.281	22.07%

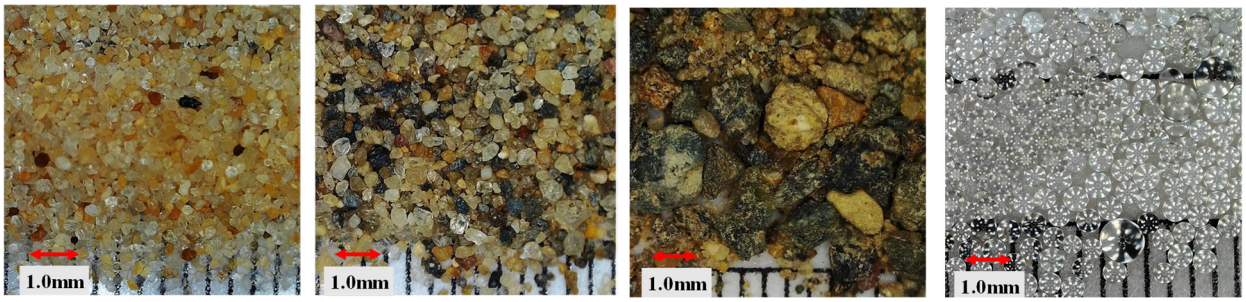

Ts (Toyoura sand) Ms1 (Mountain sand) Rs1 (River sand) Gb1 (Glass beads)

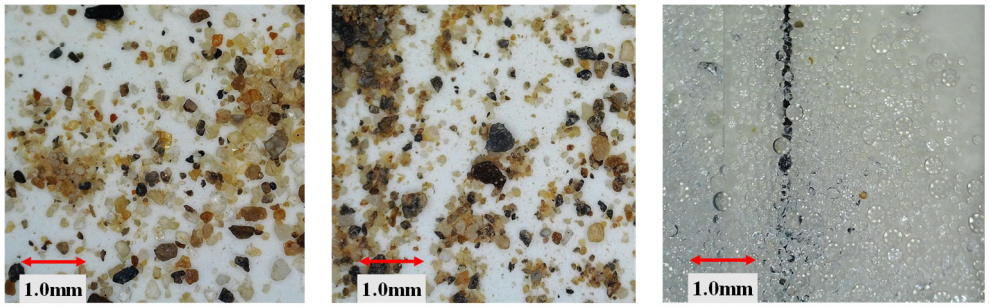

Ms2 (Mountain sand) Rs2 (River sand) Gb2 (Glass beads)

Fig. 2 Shape of sand particles in all samples.

Ms1 and Rs1, prior to the adjustment of the particle size distribution, are subject to certain larger particles. In previous studies, observations led to the assumption that river sand particles were angular in shape. In fact, the use of AR showed that the large particles in Rs1 were angular.

2.2. Testing methods

In accordance with the JIS A 1224 standards, which detail the procedures for determining the minimum and maximum densities of sands, this study employed a cylindrical mold for measurement purposes. The mold's dimensions included an inner diameter of 60 mm, a height of 40 mm, and a total volume of 113.1 cm³. The measuring technique was the emission method proposed in a previous study (Kamegaya and Nishioka, 2023).

The top surface of the mold was designed with a sharp angle, and a collar measuring 60 mm in height was positioned atop this, as shown in **Figs. 3** and **4**. In the previous study, the created slopes sometimes did not form a perfect conical shape in dense cases, and the defined measurements could not be conducted. The height of the collar was improved from 40 to 60 mm to enable defined measurements. This configuration resulted in a combined volume of 282.75 cm³ for the collar–mold assembly. This volume capacity can correspond to accommodate the

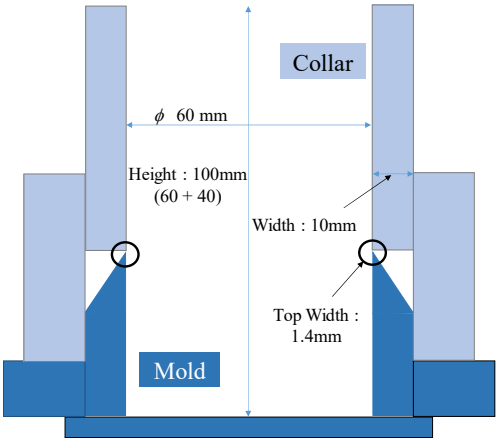

Fig. 3 Cross-sectional view of mold and collar.

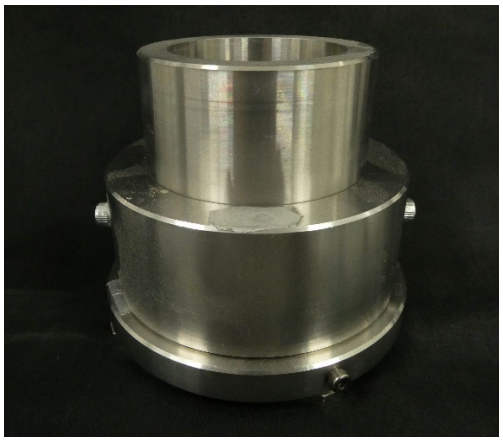

Fig. 4 Photo of mold and collar.

sample size typically retrieved by an SPT sampler. Given that the sampler penetrates to a depth of 30 cm, it covers a volume of 288.5 cm³ when factoring in the sampler's cross-sectional area. Thus, the assembly's volume is sufficient to contain a sample of at least this magnitude, making it ideal for practical applications.

Following the JIS A 1224 methodology, the sand samples were meticulously placed within the collar–mold assembly. Subsequently, the dry density (ρ_d) of each sample was precisely measured. The density conditions of the samples in the emission method were prepared in the same manner as the maximum and minimum void ratios, as specified by JIS A 1224.

Table 3 presents the average minimum density (ρ_{dmin}) values for each sample, while **Table 4** details the average maximum density (ρ_{dmax}) values. After determining the dry density (ρ_d) of the samples, a procedural step involved the careful elevation of the collar to induce a slope formation. The slope angle was characterized as the repose angle after avalanching (α_R), which was the focal point of this study, specifically under conditions of minimum density.

To quantify α_R, an assumption was made that the formed slope resembles a perfect conical shape. The apex height (h) of this cone was measured, as shown in **Fig. 5**. The bottom diameter (D_b) of the cone was determined to be 62.8 mm by adding 1.4 mm to the width of the top edge of the mold. To calculate α_R, D_b, and h were substituted into **Eq. (8)**, as shown in **Fig. 6**.

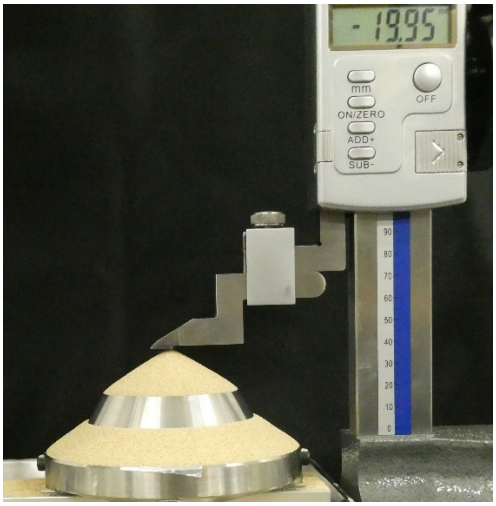

Fig. 5 Measurement of repose angle after avalanching α_R (Toyoura sand).

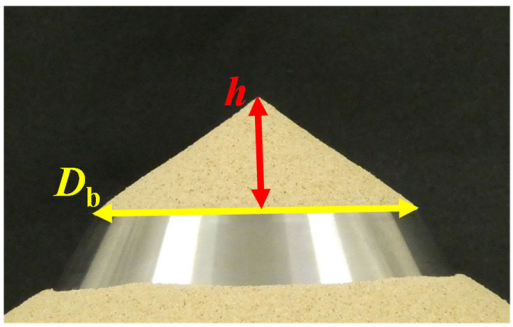

Fig. 6 Definition of the bottom diameter (D_b) and height of the apex (h) (Toyoura sand).

$$\alpha_R = \tan^{-1}\left(\frac{h}{D_b/2}\right) \tag{8}$$

Table 3 Average minimum density ρ_{dmin} (g/cm³), standard deviation(SD), and coefficient of variation(CV).

ρ_{dmin}	Ts	Ms1	Ms2	Rs1	Rs2	Gb1	Gb2
AVE	1.383	1.339	1.288	1.391	1.278	1.493	1.519
SD	0.0151	0.0015	0.0018	0.0038	0.0019	0.0026	0.0025
CV	1.093%	0.111%	0.141%	0.277%	0.150%	0.177%	0.168%

Table 4 Average maximum density ρ_{dmax} (g/cm³), standard deviation(SD), and coefficient of variation(CV).

ρ_{dmax}	Ts	Ms1	Ms2	Rs1	Rs2	Gb1	Gb2
AVE	1.649	1.609	1.603	1.687	1.605	1.593	1.785
SD	0.0226	0.0103	0.0046	0.0075	0.0040	0.0028	0.0117
CV	1.371%	0.637%	0.285%	0.445%	0.252%	0.178%	0.656%

3. Results and discussion

Fig. 7 shows the correlation between the minimum density (ρ_{dmin}) and the repose angle after avalanching (α_R) for various sand samples. In this representation, the open symbols (Ms1, Rs1, Gb1) denote the samples before particle size distribution adjustment, and the closed symbols (Ms2, Rs2, Gb2) represent the results after approximation to the particle size distribution of Ts. The α_R value for Gb1 was obtained from the study by Kamegaya and Nishioka (2023) from a test with a 40 mm collar height.

3.1. Impact of particle size distribution

This section presents a comparison of the α_R results before and after the adjustment of their particle size distributions, as shown in **Fig. 7**. The applicable samples were mountain sand (Ms1, Ms2), river sand (Rs1, Rs2), and glass beads (Gb1, Gb2).

For mountain sand (Ms1, Ms2) and river sand (Rs1, Rs2), the adjustment led to an increase in the proportion of smaller diameter particles in Ms2 and Rs2. This alteration in particle size distribution not only impacted the density but also affected the α_R. In both these samples, the gradient of the particle size distribution curve became steeper, coinciding with a trend of decreasing density and increasing α_R.

The scenario differed for the glass beads (Gb1, Gb2). For both bead types, despite considerable disparity in their particle size distributions, the α_R values were approximately 25°. Gb1, consisting of two different diameter beads, does not exhibit a smooth curve due to its minimum particle size of 0.5 mm. Conversely, Gb2, composed of four different diameter beads, presents a smoother curve. This variation in particle size distribution is analogous to that observed in the mountain and river sands. However, the glass beads demonstrate an increase in density without a notable difference in α_R. This finding suggests that the impact of particle size distribution on the angle of repose is minimal for samples with a spherical shape and low surface roughness, such as glass beads.

3.2. Impact of soil type

This section presents a comparison of the α_R results, as shown in **Fig. 7,** for Ts and three other samples with approximate particle size distributions. The applicable samples were Ts, Ms2, Rs2, and Gb2.

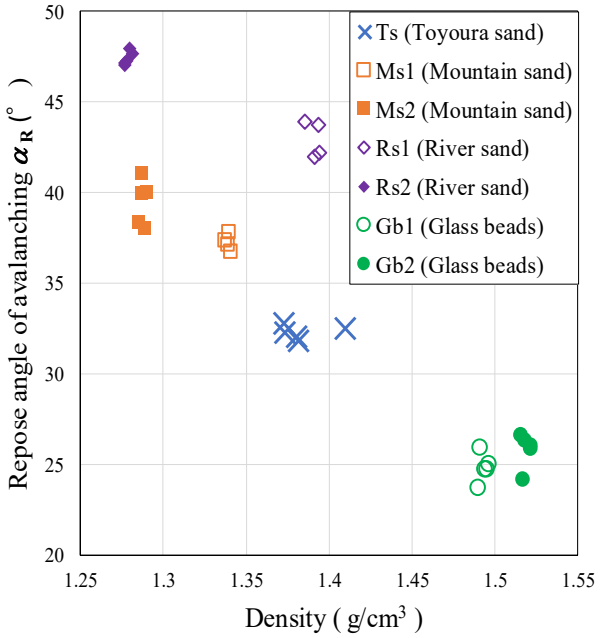

Fig. 7 Change in repose angle after avalanching α_R at minimum density with particle size distribution and particle type.

Rs2 exhibited the highest α_R, followed by Ms2, Ts, and Gb2 in descending order. Gb2, with an AR of 1.0, had the smallest α_R. The difference in α_R between the three samples with AR $\neq$ 1.0 and Gb2 exceeded 5°, indicating a clear distinction likely attributable to the influence of particle shape on α_R. The characteristic low surface roughness of glass beads is considered a contributing factor.

When comparing spherical and nonspherical samples, the spherical sample (with a lower AR) was observed to exhibit a reduced α_R. This reinforces the assumption that the rolling resistance index significantly impacts the angle of repose.

Despite similar AR values, Ts, Ms2, and Rs2 demonstrated distinct α_R values. One reason for this result may be the imperfect matching of the particle size distributions. However, the study's results suggest the presence of factors beyond particle size distribution and particle shape that influence α_R. Differences in the samples not evident from enlarged images or particle size distribution analysis, such as surface roughness and

coefficient of curvature, are assumed to affect the angle of repose. As the lower surface roughness of glass beads compared with other samples, surface roughness may have been a potential factor influencing α_R.

Overall, for all samples shown in **Fig. 7**, the order of α_R values from the highest to lowest is river sand, mountain sand, Toyoura sand, and glass beads. The range of α_R values varied for each sample type, indicating that α_R was more significantly influenced by the physical properties of the soil samples than their particle size distributions. This study demonstrates that the proposed emission method effectively captures the effects of particle size distribution, particle shape, and other influencing factors on the angle of repose.

3.3. Slope profile

Fig. 8 shows the slope profiles at minimum density for all samples. A distinct mountain slope is evident in all samples. However, an increased tendency for slope collapse was observed in Ms2 and Rs2 following particle size adjustment. This observation was made during the test process which the slope was created by delicately lifting the collar upward, and the apex of the slope was measured to determine α_R. In the cases of Ms2 and Rs2, slope collapses occurred readily under minor impacts during the testing, hindering accurate measurements. Notably, although slope instability and collapses are more commonly expected under high density conditions, they have occurred at low density conditions in our experiments.

Considering that Ms2 and Rs2 did not exhibit significant differences from Ts in terms of particle rollability, the ease of slope collapse in these samples might be attributed to factors other than particle shape. This suggests that additional variables, potentially related to the physical properties of the sand or the testing methodology, could be influencing the stability of the slopes.

4. Conclusions

In this paper, we presented a comprehensive analysis of the repose angle after avalanching (α_R) as determined by the emission method, with a particular focus on the influences of particle size distribution and shape. Our results demonstrated that α_R varies based on these two aspects, with an indication that other factors, such as surface roughness, may also play a significant role.

A key finding was the increase in α_R for mountain and river sands when their particle size distributions were adjusted to include a higher proportion of small-sized particles. By contrast, the α_R values for glass beads remained unchanged despite similar modifications to their

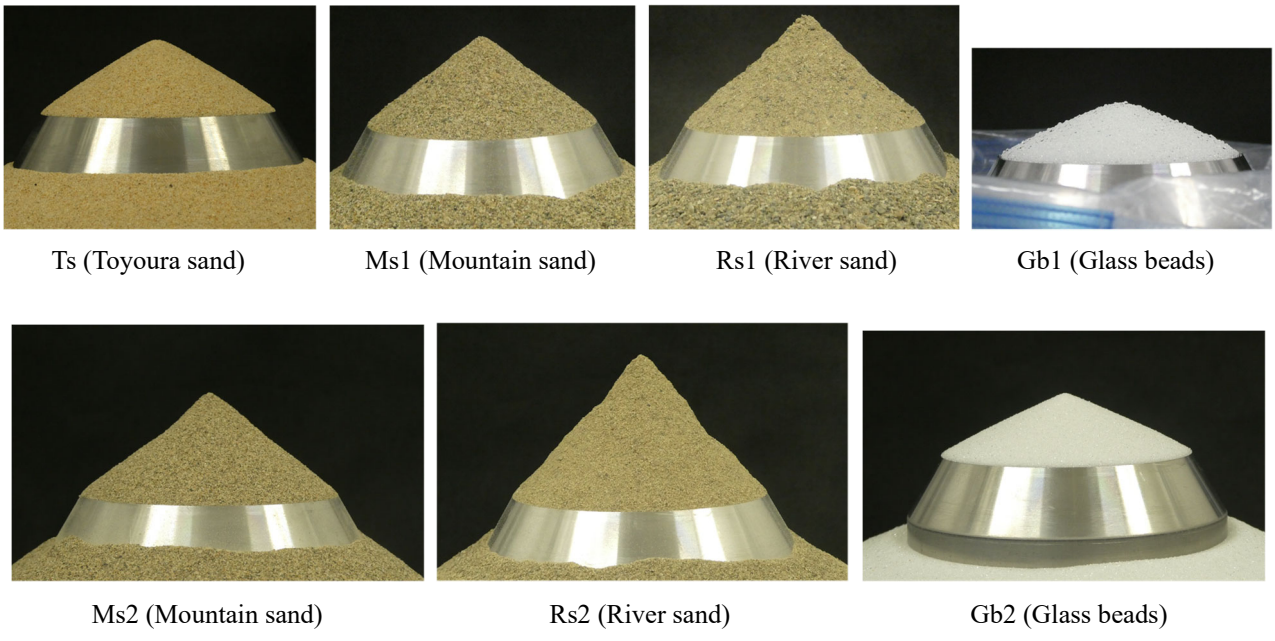

Fig. 8 Slope profile at minimum density of all samples.

particle size distributions. This suggests a minimal impact of particle size distribution on samples with spherical shapes and low surface roughness, such as glass beads.

The comparison between the spherical glass beads and other three sand samples (Toyoura, mountain, and river sands) under conditions of approximate particle size distribution revealed a notable difference. The α_R of the glass beads was consistently low, indicating the potential influence of particle shape on the angle of repose. Significant variations in α_R were also observed among Toyoura, mountain, and river sands, despite their similar AR. This highlights the likelihood of additional factors, beyond particle size distribution and shape, influencing α_R.

Our findings suggest that the physical properties of the soil samples might exert a more pronounced impact on α_R than their particle size distribution. This indicates the multifaceted nature of the emission method as a test influenced by an array of factors including density, particle size distribution, particle shape, and potentially others.

This study corroborated the variability of α_R in relation to the particle size distribution and shape, as well as its dependency on other factors such as surface roughness. Previous studies, such as that by Kamegaya and Nishioka (2023) also reported differences in the trend of α_R's increase relative to relative density (D_r) among different samples. Consequently, α_R is a potentially effective parameter for enhancing the accuracy of estimating the angle of internal friction (ϕ).

The potential of α_R is significant, opening avenues for the development of a highly accurate estimation method that integrates the physical and structural properties of soil particles. We expect that the statistical estimation of ϕ will be augmented by including α_R obtained from the emission method. This approach would offer a more comprehensive analysis than relying solely on the SPT N-value. Such an integrated method could provide more precise estimates of ϕ, thereby facilitating better planning and execution of engineering projects involving granular materials.

The results of this study show that the α_R values obtained using the emission method, along with the observed trend of α_R's increase relative to D_r, which is observed separately, indicate the basic mechanical properties of the soil particles. These indicators can be easily obtained from disturbed samples after the SPT. The current practical methods rely solely on direct statistical relationships between SPT N-values and ϕ values, neglecting key indicators of soil particle mechanical properties. Further work will aim to propose a more accurate method for estimating the ϕ values by incorporating easily obtainable indicators through multivariate analysis.

Acknowledgments

We would like to thank Editage (www.editage.com) for English language editing.

References

Architectural Institute of Japan, 2001. *Recommendations for design of building foundations* (in Japanese).

Japan Road Association, 2002. *Specifications for highway bridges*, *Part Ⅳ Substructures* (in Japanese).

Kamegaya, E. and Nishioka, H., 2023. Fundamental study of the effect of particle shape and relative density of sand on the angle of repose test results, *The 13th International Conference on Geotechnique, Construction Materials and Environment*, g13154.

Kwag J., Ochiai H., Yasufuku N., Ohno S., and Omine K., 1998. Angles of repose and shear resistance of sandy soil., *Jap. Soc. Civil Eng. 1998 Annual Meeting*, *Ⅲ-A24*, pp.48–49 (in Japanese).

Maeda, K., Moriguchi, S., Matsushima, T., Koyama, T., and Nakata, Y., 2015. 6. Parameter setting and soil and ground making Part 1 (Distinct element method for geotechnical engineering), *Soils and Found. 63, No.8*, pp.71-78 (in Japanese).

Matsukura, Y. and Onda, Y., 1989. Angle of repose: A matter of semantics and a variety of the measuring methods, *Bull. Environm. Res. Center, Univ. Tsukuba 13*, pp. 27-35 (in Japanese).

Matsuoka, H., Liu, S.H., Yamada, T., Matsuyama, K., and Yoshimura, Y., 2003. Prediction of the angle of internal friction for sands, gravels and coarse-grained soils from the grain shape and relative density, *The 38th Jap. National Conf. Geotech. Eng. D-06*, pp. 551–552 (in Japanese)

Meyerhof, G.G., 1956. Penetration Test and Bearing Capacity of Cohesionless Soils, *Proc. of ASCE*,

Journal of the Soil Mech. and Found. Div. 82, No.SM.1, p.866.

Nakata, Y., Moriguchi, S., Kajiyama, S., Kido, R., Kikkawa, N., Saomoto, H., Takano, D., and Higo, Y., 2022. Experimental data of 3D printed granular material for verification of discrete element modeling simulation, *Soils and Found. 62, No. 4*, 101178.

Railway Technical Research Institute, 2000. *Design Standards for Railway Structures and Commentary*, *Foundation structures and Soil-pressure resisting structures* (in Japanese).

Schultze, E. and Menzenbach, 1961. Standard Penetration Test and Compressibility of Soils, *Proc. of 5th ICSMFE Ⅰ*, pp.527-532.

The Japan Harbor Transportation Association, 1999. *Technical Standards for Port and Harbor Facilities 1* (in Japanese).

Yoshida, Y. and Kokusho, T., 1988. A proposal on application of penetration tests on Gravelly Soils., *CRIEP*, U87080 (in Japanese).